Light Scattering in the Course of a Polymerization-Induced Phase Separation by a Nucleation-Growth Mechanism

Guillermo E. Eliçabe,*,† Hilda A. Larrondo,‡ and Roberto J. J. Williams†

Institute of Materials Science and Technology (INTEMA, University of Mar del Plata, and National Research Council, CONICET) and Department of Physics, Faculty of Engineering, University of Mar del Plata, J. B. Justo 4302, 7600 Mar del Plata, Argentina

Received April 6, 1998; Revised Manuscript Received July 22, 1998

ABSTRACT: Polymerization-induced phase separation was described using a phase transformation diagram in conversion vs composition coordinates, where metastable and unstable regions were located. Phase separation through a nucleation-growth (NG) mechanism, in the metastable region of the phase diagram, was described with the usual constitutive equations. A distribution of particle sizes was generated as a function of conversion. Different possible composition profiles inside and outside the particles were predicted, leading to refractive index profiles associated with individual particles. Representative sets of particles were properly located in the scattering volume, and the light scattering pattern of the ensemble was generated. A maximum at a wave vector $q \neq 0$ was present in the following cases: (a) at low concentrations of dispersed-phase particles when a depletion layer surrounded the particles and (b) at high concentrations of dispersed-phase particles due to the correlation produced by the location of individual scatterers in a constrained space. Both effects generated a maximum in the scattered intensity at $q \neq 0$, even for broad particle-size distributions. The position of q_{max} increased with the concentration of dispersed-phase particles. For systems that do not exhibit coarsening effects, the light scattering peak will initially shift to the right and then grow in intensity at a constant value of the wave vector, when nucleation becomes negligible. Coarsening produces a shift of the scattering peak to the left, while increasing its intensity. Therefore, the presence of a maximum in the light scattering pattern should no longer be indicated as the hallmark of spinodal demixing, as is frequently stated in the literature.

1. Introduction

Polymerization-induced phase separation (PIPS) is a process by which an initially homogeneous solution of an unreactive component in reactive monomers becomes phase separated in the course of polymerization. The initial process of phase separation occurs via the mechanism of nucleation-growth (NG) in the metastable region of the phase diagram or by spinodal decomposition (SD) if the system becomes unstable.

The phase separation process can be followed by light scattering experiments that measure the time (t) evolution of the scattered intensity, $I(q,t)$, where q is the magnitude of the scattering wave vector, **q**. SD is characterized by the appearance of a peak in $I(q,t)$ at a particular $q_{max} \neq 0$. In most cases the intensity of the peak increases while q_{max} shifts to lower q values as phase separation proceeds. The presence of a maximum in the light scattering pattern is usually referred to as a hallmark of SD.[1−3] In contrast, if phase separation takes place by NG, it is normally expected that I peaks at $q = 0$ and then decreases monotonically until a diffraction maximum is encountered. These types of maxima are only found when either the particles are large or the measurement range in q space is broad,[4] a situation that is not of interest in this investigation. However small particles growing by an NG mechanism may still show the presence of a scattering maximum at a $q_{max} \neq 0$ in relatively narrow q ranges as we have recently shown.[5] The origin of this scattering behavior is the presence of a layer surrounding dispersed-phase particles that contains less solute concentration than the bulk (depletion layer, DL). As the solute segregated to the dispersed particles was originally contained in the DL, the external region keeps the initial solute concentration. This picture is constrained to the generation of a diluted dispersion and may be only used in the initial stages of a PIPS. The aim of this publication is to complement the previous one[5] by extending the analysis to the whole range of the phase separation process occurring by an NG mechanism. We will show that a maximum in light scattering at $q_{max} \neq 0$ may be also expected by the presence of a spatial correlation[6] effect always present at high volume fractions of particles even for broad distributions of particle sizes. Therefore, the presence of a maximum in $I(q,t)$ at $q_{max} \neq 0$ should not be automatically ascribed to the presence of SD.

The manuscript is organized as follows. First a model of phase separation by nucleation and growth will be discussed. It will enable us to locate metastable and unstable regions in a phase transformation diagram and to predict the evolution of the particle-size distribution in the course of polymerization along the metastable region. The NG model is basically the same as that used to predict the distribution of dispersed-phase particles in rubber-modified thermosets.[7−9] To analyze the effect of polydispersity in the particle-size distribution, a simplified version of the NG model that generates monodisperse distributions will be also used. As the model only predicts the evolution of average compositions in both dispersed and continuous phases, in a subsequent section different possible composition profiles inside and outside the particles will be considered. This leads to refractive index profiles associated with individual particles. Then, representative sets of par-

†INTEMA.
‡Department of Physics.

10.1021/ma9805304 CCC: $15.00
Published on Web 10/30/1998

ticles present at different conversions in the polymerization reaction will be used to partially fill the scattering volume. Then the light scattering pattern of the ensemble will be generated. Factors leading to the presence of a maximum in the intensity of the scattered light at $q_{max} \neq 0$, will be discussed.

2. Model of Phase Separation by Nucleation and Growth

2.1. Phase Transformation Diagram. To obtain the particle-size distribution along the polymerization, it is first necessary to generate a phase transformation diagram showing stable, metastable and unstable regions.

For illustration purposes we will consider a pseudobinary system consisting of a solution of a rubber (component 2) in a stoichiometric diepoxy (B2)−diamine (A4) reactive solvent (component 1). The Flory−Huggins equation may be used to describe the free energy of mixing per unit volume:

$$\Delta G = (RT/\bar{V}_{10})[(\phi_1/z_1) \ln \phi_1 + (\phi_2/z_2) \ln \phi_2 + \chi\phi_1\phi_2] \quad (1)$$

where R is the gas constant, T is the absolute temperature, χ is the interaction parameter, ϕ_1 and ϕ_2 are, respectively, the volume fraction of thermoset (epoxy−amine) and rubber, and $\bar{V}_{10}$ is the initial molar volume of the thermoset defined as

$$\bar{V}_{10} = \bar{M}_{n,10}/\rho_1 \quad (2)$$

The mass density of the reactive solvent, ρ_1, is assumed constant and its number average molar mass is given by

$$\bar{M}_{n,10} = (M_{A4} + 2M_{B2})/3 \quad (3)$$

The ratios of molar volumes are defined as

$$z_1 = \bar{V}_1/\bar{V}_{10} = \bar{M}_{n,1}/\bar{M}_{n,10} = 1/(1 - 4p/3) \quad (4)$$

$$z_2 = \bar{V}_2/\bar{V}_{10} \quad (5)$$

While z_2 remains constant along polymerization, z_1 increases with conversion p (eq 4 is valid in the pregel stage of the A4 + B2 step polymerization in the absence of intramolecular cycles).

A typical rubber-modified epoxy−amine system is selected,[8] with the following values for the parameters defined in eq 1: $\bar{V}_{10} = 277.1$ cm^3/mol, $z_2 = 13.9$, and

$$\chi = 0.336 + 69.457/T \quad (6)$$

A temperature $T = 393$ K is selected to illustrate the system's behavior.

Binodal and spinodal curves are obtained from eq 1 following usual procedures.[7−9] Figure 1 shows the resulting phase transformation diagram in conversion vs volume fraction coordinates, up to the gel conversion ($p_{gel} = 0.6$). It may be assumed that most of the phase separation process takes place in the pregel region.[7−9]

2.2. Distribution of Particle Sizes. As shown in Figure 1, starting from an initial volume fraction (composition) ϕ_{20}, the system enters the metastable region at the cloud-point conversion (p_{cp}) located on the binodal curve. Once in this region, phase separation may proceed through an NG mechanism. The evolution

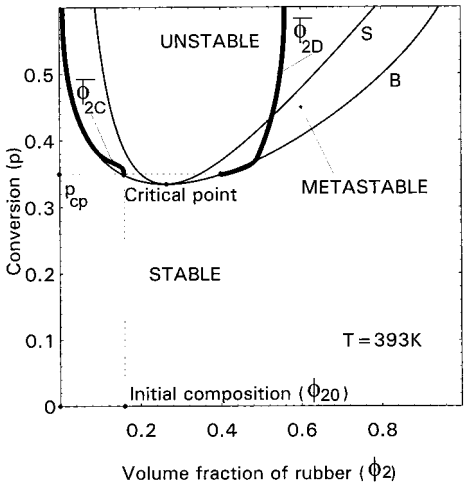

Figure 1. Binodal (B) and spinodal (S) curves in a conversion vs composition transformation diagram at $T = 393$ K. The critical point and the location of stable, metastable and unstable regions are shown. A predicted trajectory arising from a nucleation-growth phase separation mechanism is plotted. $\bar{\phi}_{2c}$ indicates the average rubber composition remaining in the continuous phase, while $\bar{\phi}_{2D}$ means the average rubber composition in the dispersed phase. $\phi_{2\alpha}$ and $\phi_{2\beta}$ are the equilibrium compositions. ϕ_{20} is the initial composition, and p_{cp} is the cloud-point conversion.

of the average composition of continuous and dispersed phases, $\bar{\phi}_{2c}$ and $\bar{\phi}_{2D}$ is determined by the competition between phase separation and polymerization rates.

A model describing the evolution of morphological parameters (concentration of dispersed-phase particles, particle-size distribution, volume fraction of dispersed phase), together with average compositions of continuous and dispersed phases, is available in the literature.[7−9] It will be used to generate the distribution of particle sizes along conversion for the particular system under study. Only the most relevant features of the model will be described in what follows.

The nucleation rate is expressed by

$$dN_T/dt = N_0 D \exp(-\Delta G_{cr}/kT) \quad (7)$$

where N_T is the volumetric concentration of particles (generated with a critical radius R_{cr}), D is the diffusion coefficient of the rubber in the thermoset, which depends on conversion, N_0 is an adjustable parameter, k is the Boltzmann constant and ΔG_{cr} is the free energy barrier necessary to overcome formation of nuclei of critical radius R_{cr}. ΔG_{cr} and R_{cr} may be calculated with the following expressions:

$$\Delta G_{cr} = 16\pi\sigma^3/(3|\Delta G_N|^2) \quad (8)$$

$$R_{cr} = 2\sigma/|\Delta G_N| \quad (9)$$

where ΔG_N is the free energy change per unit volume associated with the phase separation process (calculated from the Flory−Huggins equation[7−9]), and σ is the interfacial tension given by[10]

$$\sigma(mN/m) = 0.153(z_2/z_1)^{0.5}(\phi_{2N} - \bar{\phi}_{2C})^{3.85} \quad (10)$$

ϕ_{2N} is the instantaneous composition of the segregated phase at a particular conversion p (calculated from the Flory−Huggins equation[7−9]), and $\bar{\phi}_{2c}$ is the average volume fraction of the rubber remaining in the continuous phase at the same conversion (Figure 2). In fact, it

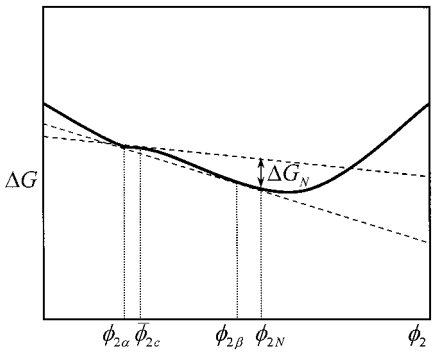

Figure 2. Free energy of mixing per unit volume as a function of rubber volume fraction for a particular conversion in the metastable region; $\phi_{2\alpha}$ and $\phi_{2\beta}$ are the equilibrium compositions, $\bar{\phi}_{2c}$ is the actual average composition of the continuous phase, ϕ_{2N} represents the instantaneous composition of the segregated phase, and ΔG_N is the free energy change per unit volume associated with the phase separation process (maximum difference between the ΔG curve and the straight line that is tangent to this curve at $\bar{\phi}_{2c}$).

is the low values of interfacial tensions predicted by eq 10 that makes phase separation by an NG mechanism possible.[9]

For the particular system under study, the following values were taken: $N_0 = 1.54 \times 10^{16}$ cm^{-5} and

$$D = \frac{D_0 T}{\eta} \tag{11}$$

where $D_0 = 10^{-11}$ cm^2 s^{-1} Pa s K^{-1} and

$$\eta = 0.1\left(1 - \frac{p}{p_{gel}}\right)^{-2.5} \text{(Pa s)} \tag{12}$$

The viscosity of the continuous phase, η, increases with conversion becoming infinite at p_{gel}. Equation 12 approximately fits the experimental behavior for the particular system under consideration;[8] N_0 and D_0 have the same values as those previously used for the same system.[8]

When the system evolves through the metastable region, particle growth occurs because of the driving force ($\bar{\phi}_{2c} - \phi_{2\alpha}$) which tries to restore the system to equilibrium conditions.

The differential volume increase of a generic particle of radius R_i may be written as

$$\frac{4\pi \mathrm{d}R_i^3}{3\ \mathrm{d}t} = k_{\phi i}(4\pi R_i^2)(\bar{\phi}_{2c} - \phi_{2\alpha}) \tag{13}$$

where $k_{\phi i}$ is the mass transfer coefficient given by[7-9]

$$k_{\phi i} = \frac{D}{R_i} \tag{14}$$

From eqs 13 and 14, the growth-rate law for a generic particle may be derived:

$$R_i \frac{\mathrm{d}R_i}{\mathrm{d}t} = D(\bar{\phi}_{2c} - \phi_{2\alpha}) \tag{15}$$

Using the available experimental equation for the polymerization kinetics of the particular diepoxide−diamine system,[11] it is possible to replace time (t) by conversion (p), thus expressing the evolution of morphological parameters as a function of conversion. The following parameters may be obtained by solving the NG equations: $N_i(R_i)$ (distribution of particle sizes), N_T (total particle concentration), V_D (volume fraction of dispersed phase), and $\bar{\phi}_{2D}$ (average rubber volume fraction in the dispersed phase). The average rubber composition in the continuous phase, $\bar{\phi}_{2c}$, is obtained from the following mass balance:

$$\phi_{20} = (1 - V_D)\bar{\phi}_{2c} + V_D\bar{\phi}_{2D} \tag{16}$$

A simplified version of this model, leading to a monodisperse distribution of particle sizes, $N_T(R)$, may be generated. In this case, it is the differential increase in the volume fraction of dispersed phase that is calculated:

$$\frac{\mathrm{d}V_D}{\mathrm{d}t} = \frac{4\pi}{3}R_{cr}^3\frac{\mathrm{d}N_T}{\mathrm{d}t} + k_\phi 4\pi R^2 N_T(\bar{\phi}_{2c} - \phi_{2\alpha}) \tag{17}$$

Solving eqs 7 and 17 leads to V_D and N_T as a function of conversion. R arises from

$$R = \left(\frac{3V_D}{4\pi N_T}\right)^{1/3} \tag{18}$$

Regarding the average composition of dispersed phase particles, it is observed in Figure 1 that $\bar{\phi}_{2D}$ becomes relatively distant from the equilibrium value $\phi_{2\beta}$ because no mass is allowed to return to the continuous phase (the epoxy−amine species are assumed to remain trapped in the rubbery-rich dispersed phase particles). But as the $\bar{\phi}_{2D}(p)$ trajectory enters the metastable (and even unstable) region, a secondary phase separation may (must) take place inside dispersed domains. To account for this possibility in the light scattering model, two extreme cases will be considered in the following section: (a) homogeneous particles with composition $\bar{\phi}_{2D}(p)$, meaning that secondary phase separation produces such a fine dispersion that the particle appears homogeneous at the wavelength of visible light; (b) bilayer particles consisting of a rich-thermoset core (radius R_{ci}, composition $\phi_{2\alpha}$) surrounded by a rubbery shell (thickness $R_i - R_{ci}$, composition $\phi_{2\beta}$). Both $\phi_{2\alpha}$ and $\phi_{2\beta}$ are the equilibrium compositions for the particular conversion p; R_{ci} is determined by a mass balance giving $\bar{\phi}_{2D}$ as the average composition of the particle. A secondary phase separation inside dispersed phase particles has been frequently reported in the literature.[12]

Composition profiles outside dispersed phase particles may be also considered, as discussed in the next section.

3. Composition Profiles Inside and Outside Particles

The model of the previous section provides us with variables that partially supply the information needed to calculate the light scattering profiles of the growing particles. This information can be completed in part by defining the composition profiles inside and outside the particles.

Inside the particles, two possibilities are considered. First, one in which two new phases are segregated, forming a core rich in thermoset and a shell rich in rubber (bilayer particles). The second one considers the particles as homogeneous.

Outside the particles, three cases are considered. The first takes into account that the medium, i.e., the continuous phase, is homogeneous. The second consid-

ers that the particles grow at the expense of a depletion layer that surrounds them. This last situation is only possible if a very diluted dispersion of particles is considered. When the concentration of particles grows, the formation of a depletion layer is no longer possible because the particles are too close to each other. In that case one should expect the formation of a complicated contour of concentrations, which depends now not only on the mass balances around each particle but also on the distribution of the growing particles in space. In this work this complex situation will not be further addressed. Instead, the effect of a thin film surrounding the particles containing less rubber composition than the bulk will be analyzed for the case in which the volume fraction of particles is high enough to preclude the formation of a real depletion layer.

The combination of these different alternatives for the composition profiles gives rise to a number of cases that could be studied. Only four of the possible alternatives will be considered here: homogeneous particles in a homogeneous medium, homogeneous particles with a depletion layer, homogeneous particles with an arbitrary coating film, and bilayer particles in a homogeneous medium.

3.1. Homogeneous Particles. If the medium is also homogeneous, the average rubber composition in the medium, $\bar{\phi}_{2c}$, together with the average rubber composition in the particle, $\bar{\phi}_{2D}$, is all one needs to calculate the refractive indices in both phases,

$$n_0 = \bar{\phi}_{2c} n_A + (1 - \bar{\phi}_{2c}) n_B \tag{19}$$

$$n_p = \bar{\phi}_{2D} n_A + (1 - \bar{\phi}_{2D}) n_B \tag{20}$$

where n_0 and n_p are the refractive indices of medium and particle, respectively, and n_A and n_B are the refractive indices of rubber and thermosetting polymer, respectively (for the present study the following values were taken: $n_A = 1.49$, $n_B = 1.61$).

When either a coating film or a depletion layer is present, the average composition of the rubber in the medium is the result of averaging a composition profile in which the rubber composition is lower than the average close to the particle and higher far from it.

Assume that the particle-size distribution at any arbitrary conversion p, may be represented by a set of N pairs, N being the number of different sizes present in the distribution, including the particle radius, R_i, and the corresponding number of particles per unit volume of sample, N_i, for each size. This leads to the following expression for the volume fraction of particles in the sample

$$V_D = \frac{4}{3}\pi \sum_{i=1}^{N} N_i R_i^3 \tag{21}$$

Assume also that a coating film of thickness $(R_{di} - R_i)$ is enclosing particle i, where R_{di} is in principle arbitrary.

The rubber concentration profile outside the particle, $\phi_{2i}(r)$, follows a hyperbolic profile arising from the solution of the differential mass balance:[5]

$$\frac{\phi_{2c} - \phi_{2i}}{\phi_{2c} - \phi_{2\alpha}} = \left(\frac{\frac{1}{r} - \frac{1}{R_{di}}}{\frac{1}{R_i} - \frac{1}{R_{di}}} \right) \tag{22}$$

where $\phi_{2\alpha}$ is the equilibrium rubber composition at $r = R_i$ (at the particular conversion p) and ϕ_{2c} is the particular rubber composition for $r \geq R_{di}$ ($\phi_{2c} > \bar{\phi}_{2c}$).

The average rubber composition in the coating films of all particles, $\bar{\phi}_{2(coat)}$, may be obtained by integrating eq 22:

$$\bar{\phi}_2(\text{coat}) = \phi_{2c} - (\phi_{2c} - \phi_{2\alpha}) \frac{\sum_{i=1}^{N} N_i (R_{di}^2 R_i + R_i^2 R_{di} - 2R_i^3)}{2 \sum_{i=1}^{N} N_i (R_{di}^3 - R_i^3)} \tag{23}$$

The following mass balance of rubber holds:

$$\left[1 - \frac{4}{3}\pi \sum_{i=1}^{N} N_i R_i^3\right] \bar{\phi}_{2c} = \left[\frac{4}{3}\pi \sum_{i=1}^{N} N_i (R_{di}^3 - R_i^3)\right] \bar{\phi}_2(\text{coat}) + \left[1 - \frac{4}{3}\pi \sum_{i=1}^{N} N_i R_{di}^3\right] \phi_{2c} \tag{24}$$

from which ϕ_{2c} may be obtained.

If n_0 is now the refractive index of the medium outside the coatings, eq 19 can still be used with $\bar{\phi}_{2c}$ replaced by ϕ_{2c}. Inside the coatings the refractive index is now a function of radius, r, which may be calculated from eqs 19, 20, and 22:

$$n_{di}(r) = n_A \phi_{2i}(r) + n_B [1 - \phi_{2i}(r)] = n_0 + (n_0 - n_p) \frac{(\phi_{2c} - \phi_{2\alpha})}{(\bar{\phi}_{2D} - \phi_{2c})} \frac{\left(\frac{1}{r} - \frac{1}{R_{di}}\right)}{\left(\frac{1}{R_i} - \frac{1}{R_{di}}\right)} \tag{25}$$

Until now the thickness of the coating has been selected arbitrarily. If, instead, a depletion layer (to the expense of which the particles grow) is considered, the thickness of this layer can no longer be arbitrary. By applying the mass conservation principle, we obtain

$$R_{di} = \frac{1}{2}\left\{\left[9 + 8\left(\frac{\bar{\phi}_{2D} - \phi_{2c}}{\phi_{2c} - \phi_{2\alpha}}\right)\right]^{1/2} - 1\right\} R_i \tag{26}$$

In this case ϕ_{2c} is equal to ϕ_{20}.

Figure 3 schematically represents the different cases analyzed here for homogeneous particles.

3.2. Bilayer (Core−Shell) Particles. Only the case in which the medium is homogeneous will be considered here. In the core and shell model the composition of the core and shell are $\phi_{2\alpha}$ and $\phi_{2\beta}$, respectively. Using a mass balance around the particle, the radius of the particle core, R_{ci}, can be calculated as a function of the average composition in the particle, $\bar{\phi}_{2D}$:

$$R_{ci} = R_i \left[\frac{\bar{\phi}_{2D} - \phi_{2\beta}}{\phi_{2\alpha} - \phi_{2\beta}}\right]^{1/3} \tag{27}$$

As before, n_0 is given by eq 19; the refractive index of the shell, $n_p^{(s)}$, is given by eq 20 with $\bar{\phi}_{2D}$ replaced by

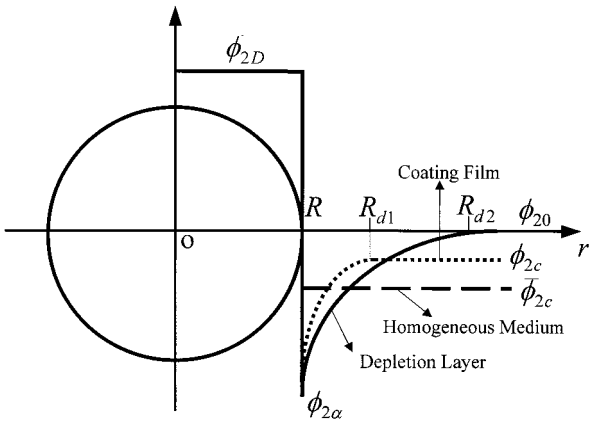

Figure 3. Schematic diagram of the composition profiles surrounding a homogeneous particle of radius R for different cases: (i) homogeneous medium; (ii) depletion layer of thickness ($R_{d2} - R$); (iii) coating film of thickness ($R_{d1} - R$).

$\phi_{2\beta}$; and the refractive index of the core, $n_p^{(c)}$, is given by eq 20 with $\bar{\phi}_{2D}$ replaced by $\phi_{2\alpha}$.

4. Distribution of Particles in Space

When the volume fraction of particles in the system under study is such that the position of the growing particles is no longer uncorrelated, the resulting light scattering pattern will be highly dependent on how the particles are arranged in space. A model to predict light scattering patterns of rather concentrated systems must include not only the information of the individual particles with regard to shape and refractive index profiles but also the information required to have a complete picture of the relative positions of the particles in the ensemble.

The model proposed here considers that the positions of the particles in the sample are selected randomly from the allowed sites. As particles fill the sample, the number of allowed sites is reduced, increasing the correlation between the centers' positions. The shape of the sample is assumed to be a square slab of thickness $2R_{max}$ and side l, where R_{max} is the radius of the largest particle. It is also assumed that the centers of the particles are all on the same plane. This last assumption reduces the computational load because, in terms of relative positions, the problem becomes bidimensional, while it keeps a three-dimensional nature in regard to the individual particles.

The particle-size distribution, $N_i(R_i)$, obtained from the phase separation model is needed to completely specify the sample. If N_p is the number of particles used to perform the computations with the model and $N_T = \sum_{i=1}^{N} N_i$ is the total number of particles per unit volume of sample, then

$$l = \left(\frac{N_p}{2R_{max}N_T}\right)^{1/2} \tag{28}$$

Note that N_p can be arbitrarily selected. However, it should be high enough to make the sample statiscally representative and low enough to make the computations feasible.

The last step is to build the sample by allocating into the volume defined for the sample, $N_i N_p / N_T$, particles of radius R_i, for $i = 1, ..., N$.

5. Light Scattering Profiles

The light scattered by an arrangement of N_p spheres immersed in a homogeneous medium illuminated by incident light of wavelength λ_0 and intensity I_i is given by[13]

$$I_s(\theta,\phi) \sim |\sum_{i=1}^{N_p} F_i(q) e^{-j\mathbf{q}\cdot\mathbf{r}_i}|^2 I_i \tag{29}$$

where $\mathbf{q} = \mathbf{q}_f - \mathbf{q}_0$, $\mathbf{q}_f$ being a vector of magnitude $(2\pi/\lambda_0)n_0$ that points from the center of each particle to the point where scattered light is detected and $\mathbf{q}_0$ a vector of magnitude $(2\pi/\lambda_0)n_0$ that points in the direction of the incident light, q is the magnitude of $\mathbf{q}$ ($q = |\mathbf{q}| = (4\pi/\lambda_0)n_0 \sin(\theta/2)$, θ and ϕ are the angles that determine the coordinates of the point where the scattered light is detected, $\mathbf{r}_i$ is the position vector of the center of particle i, j is the imaginary number, and $F_i(q)$ is the form factor of the individual particles.

For elastic single scattering by particles with spherical symmetry the form factor can be calculated as

$$F(q) = \frac{1}{q}\int_0^{R_d}[n(r) - n_0]r \sin qr \, dr \tag{30}$$

where $n(r)$ is the refractive index profile inside the particle. Note that the particle includes, in general, any layer surrounding the real particle.

Equation 29 can be arranged for calculations as

$$I_s(\theta,\phi) \sim \{(\sum_{i=1}^{N_p} F_i(q)\cos\alpha_i)^2 + (\sum_{i=1}^{N_p} F_i(q)\sin\alpha_i)^2\} I_i \tag{31}$$

with

$$\alpha_i = \mathbf{q}\cdot\mathbf{r}_i = -\frac{2\pi}{\lambda_0}(x_i \cos\phi + y_i \sin\phi)\sin\theta \tag{32}$$

where x_i and y_i are the components of vector $\mathbf{r}_i$.

For the multilayered spheres described in the previous sections, the form factors can be calculated using eq 30 and eventually eq 25:

Homogeneous Particles

$$\text{Homogeneous medium:} \quad F_i(q) = (n_p - n_0)R_i^2 \frac{j_1(qR_i)}{q} \tag{33}$$

Coating film or depletion layer:

$$F_i(q) = (n_p - n_0)\left[(1-\gamma_i)R_i^2 \frac{j_1(qR_i)}{q} + \gamma_i R_{di}^2 \frac{j_1(qR_{di})}{q} + \gamma_i R_{di}\frac{(\cos qR_{di} - \cos qR_i)}{q^2}\right] \tag{34}$$

with

$$\gamma_i = \frac{(\phi_{2c} - \phi_{2\alpha})R_i}{(\phi_{2\beta} - \phi_{2c})(R_{di} - R_i)} \tag{35}$$

$$j_1(\rho) = \frac{(\sin\rho - \rho\cos\rho)}{\rho^2} \tag{36}$$

Bilayer (Core−Shell) Particles

Homogeneous medium:

$$F_i(q) = (n_p^{(c)} - n_p^{(s)})R_{ci}^2 \frac{j_1(qR_{ci})}{q} + (n_p^{(s)} - n_0)R_i^2 \frac{j_1(qR_i)}{q} \quad (37)$$

These formulas have been derived in the past by other authors. In his book, Kerker[14] presents a complete discussion about form factors of objects with spherical symmetry, which contains the cases analyzed here.

Note that in the particular case of identical particles $F_i(q)$ is a common factor in eq 29 that gives

$$I_s(\theta,\phi) \sim |F(q)|^2 |S(q)|^2 I_i \quad (38)$$

where

$$S(q) = \sum_{i=1}^{N_p} e^{-j\mathbf{q}\cdot\mathbf{r}_i} \quad (39)$$

is the structure factor that contains the information about correlation between the centers' positions. If these positions are totally uncorrelated, as is the case in diluted systems, this structure factor tends to N_p, the number of scatterers, and only the information concerning the form factor of each particle appears in the light scattering pattern, as will be shown.

When the particles are polydisperse, the separation indicated in eq 38 is no longer possible and eq 29 must be used. Despite this fact, the two length scales corresponding to particle mean size and mean distance between centers still appear in the light scattering pattern.

To have I vs q plots as normally reported, the computations performed with eq 31 were averaged over the ϕ coordinate and smoothed along the θ coordinate as follows:

$$\langle I(\theta_k)\rangle_f = \frac{1}{2l^2 R_{max}} \frac{1}{N_\phi} \sum_{i=k-N_F}^{k+N_F} \sum_{j=1}^{N\phi} I_s(\theta_i,\phi_j) \quad (40)$$

All the reported light scattering patterns were calculated using eq 40 after selecting a proper number of ϕ's (N_ϕ) and a smoothing range $2N_F\Delta\theta$, where $\Delta\theta$ is the step in the θ coordinate. The averaged-smoothed patterns were also normalized to express them per unit scattering volume.

6. Results and Discussion

The phase separation model has been solved for two different values of ϕ_{20} (0.0497 and 0.1595). For ϕ_{20} = 0.1595 a high concentration of particles is obtained at the end of the phase separation process. For ϕ_{20} = 0.0497 the concentration of dispersed phase particles remains low during the whole conversion range.

6.1. High Concentration of Particles. This case is represented by a formulation with ϕ_{20} = 0.1595.

6.1.1. Monodisperse Particles. The simplified version of the phase separation model that considers the particles as monodisperse will be considered first. Figure 4a shows the predicted trajectory in the conversion vs composition transformation diagram while parts b and c of Figure 4 represent the evolution of volume fraction of the dispersed phase, particle concentration, and particle radius. It is observed that the trajectory lies very close to the binodal curve in the whole conversion range.

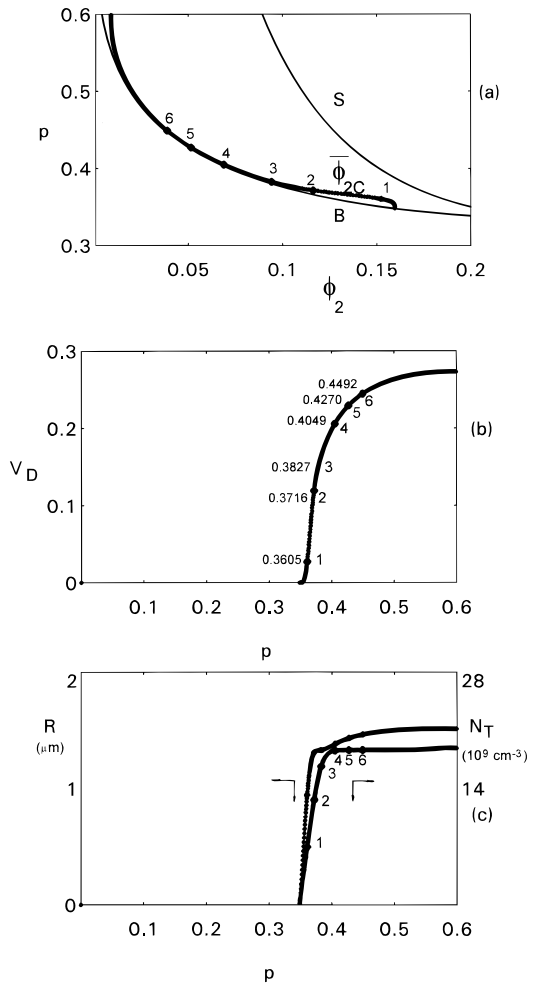

Figure 4. Predictions of the phase separation model for the case of a monodisperse distribution of particle sizes and ϕ_{20} = 0.1595: (a) evolution of the average composition in the continuous phase; (b) volume fraction of dispersed phase as a function of conversion; (c) particle concentration, N_T (cm^{-3}) and particle radius, R (μm), as a function of conversion.

Low Conversions. At the very early stages of phase separation the concentration of particles is very low and the formation of a depletion layer is likely to occur. Figure 5 shows the evolution of the light scattering profiles in that condition. The particles are assumed to be homogeneous and consequently the form factor used is that of eq 34. The light scattering profiles show a maximum at a wave vector different from zero. This maximum slightly shifts to the left as conversion increases and particle radius grows. The volume fraction of dispersed phase particles is very low during this stage and then the particles behave as if they were independent scatterers. This can be verified by calculating the light scattered by a single particle. The pattern so calculated follows almost exactly the light pattern calculated for the ensemble, except close to the origin. In that direction the light scattered by the ensemble is always coherent and then the interference peak must appear independently of the volume fraction of particles.[15] This result is also shown in Figure 5. From above, it can be concluded that the maximum in the light pattern is only a consequence of the presence of the depletion layer.

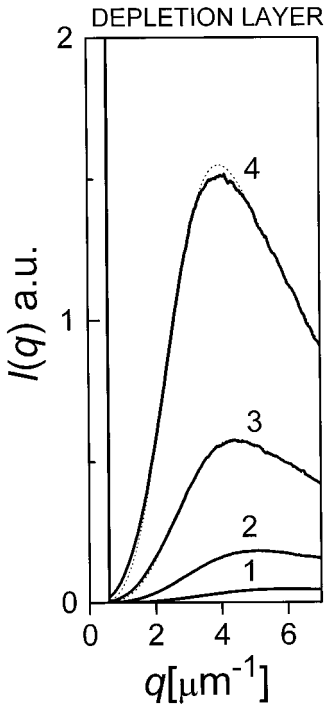

Figure 5. Evolution of the light scattering profiles (—) for the case of a monodisperse distribution of particle sizes with $\phi_{20} = 0.1595$, low conversions, and low volume fraction of particles: (1) $p = 0.3512$, (2) $p = 0.3517$, (3) $p = 0.3521$, and (4) $p = 0.3526$. Single particle model (···).

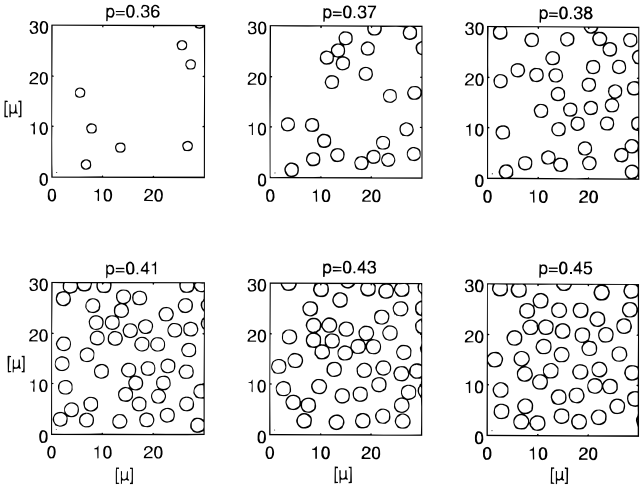

Figure 6. Evolution in real space of the sample for the case of a monodisperse distribution of particle sizes with $\phi_{20} = 0.1595$, high conversions, and high volume fraction of particles, for six different values of conversion.

For this particular case (i.e., diluted dispersion of monodisperse spheres with depletion layers exhibiting an hyperbolic variation of the refractive index), similar calculations previously performed by Tromp and Jones[16] showed the same type of results.

High Conversions. At high conversions the volume fraction of particles grows to values in which the spatial correlation among particles becomes important. In Figure 6 the evolution in real space of part of the sample that is being studied is shown for six values of conversion. These values, which cover the whole range of high conversions, correspond to stages 1−6 indicated in Figure 4. The light scattering patterns are shown in Figure 7 for different cases. Figure 7a shows the profiles for the case of homogeneous particles in a homogeneous medium (form factor of eq 33). Figure 7b shows the profiles for the case of bilayer particles in a homogeneous medium (form factor of eq 37). Figure 7c shows the profiles for the case of homogeneous particles surrounded by a coating film of thickness $R_{di} - R_i = 0.05R_i$ (form factor of eq 34).

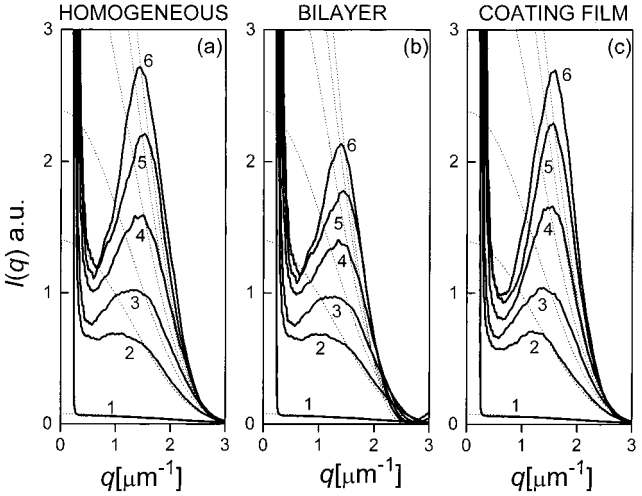

Figure 7. Evolution of the light scattering profiles (—) for the case of a monodisperse distribution of particle sizes with $\phi_{20} = 0.1595$, high conversions, and high volume fraction of particles for six different values of conversion as in Figure 6 for the following models: (a) homogeneous, (b) bilayer, and (c) coating film. Single particle model (···).

In all cases a maximum in the light intensity at a wave vector other than zero is observed. This maximum can only be attributed to the correlation effect among particles, because the light profiles corresponding to a single particle are in all cases monotonically decreasing, as shown on the same figures.

The position of the maxima in the light scattering profiles is consistent with the values that can be calculated for the much simpler problem of interference by an ordered collection of slits using $\sin \theta_{max}, = \lambda_0/(n_0 d)$ where $d = l/\sqrt{N_p}$ is the mesh size of a grid of side l where N_p particles are regularly arranged. For example, if this simple calculation is performed for the pattern of Figure 7a labeled with 6, a value of $q_{max} = 1.46\ \mu^{-1}$ is obtained. This value is in good agreement with the $q_{max} = 1.42\ \mu^{-1}$ obtained from the same figure. As d is proportional to $1/\sqrt{N_T}$, it is also clear that the position of the maxima $q_{max} = (4\pi n_0/\lambda_0) \sin(\theta_{max}/2)$ shifts to the right as N_T increases. This effect is observed in Figure 7 during the first instants in which N_T slightly increases. As the volume fraction of particles increases, the ensemble becomes more organized increasing the correlation among the positions of their centers in the scattering volume. This fact is evident in Figure 7, in which the interference maximum, a sign of order, becomes more acute as the volume fraction of particles increases. While the volume fraction of particles increases, the light intensity also increases for all wave vectors. This is in direct relation to a concurrent increase in particle size and refractive index contrast.

The main difference between the various models for the particle and surrounding medium is that at a given conversion the ratios of the maximum to the first minimum are different. The highest ratio corresponds to the model with coating film, a smaller ratio results for the homogeneous model, the smallest being the one associated with the bilayer particle model. The first

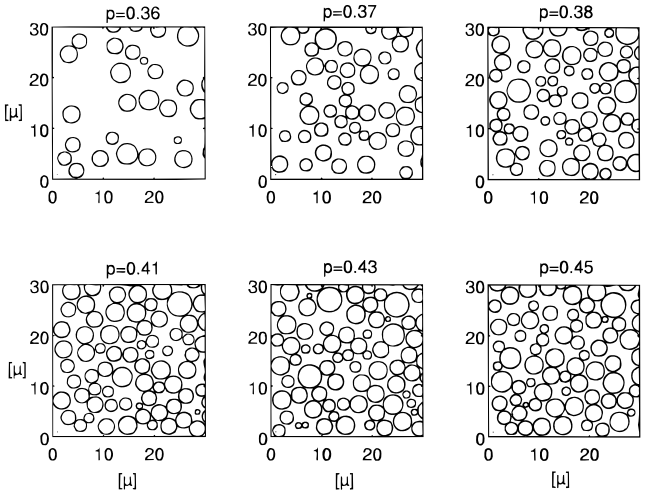

Figure 8. Evolution in real space of the sample for the case of a polydisperse distribution of particle sizes with $\phi_{20} = 0.1595$, high conversions, and high volume fraction of particles, for six different values of conversion.

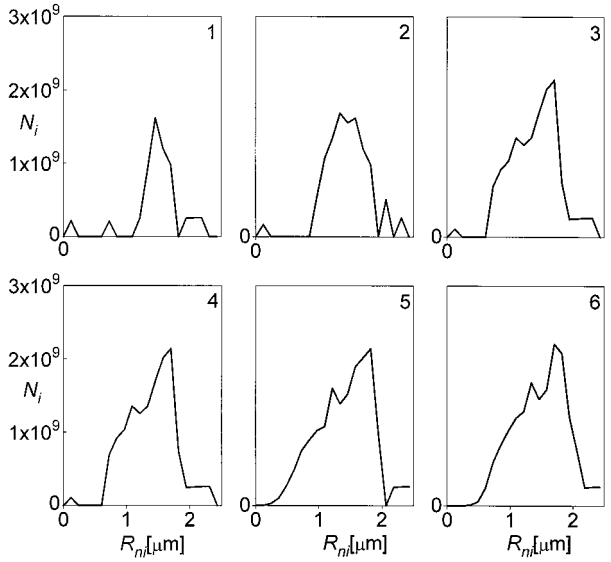

Figure 9. Particle-size distributions corresponding to Figure 8.

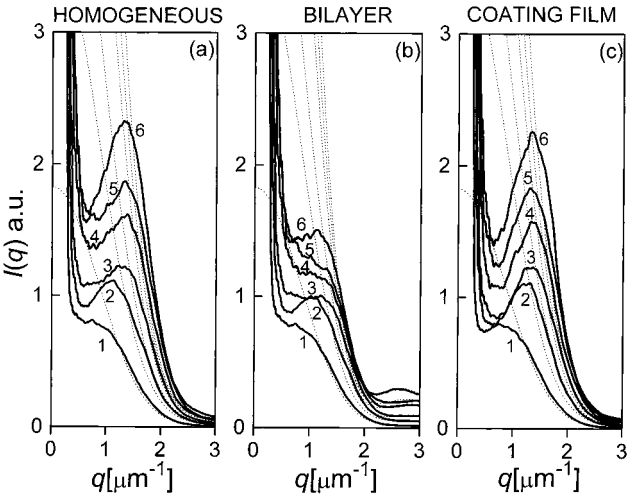

Figure 10. Evolution of the light scattering profiles (—) for the case of a polydisperse distribution of particle sizes with $\phi_{20} = 0.1595$, high conversions and high volume fraction of particles for six different values of conversion as in Figure 8 for the following models: (a) homogeneous, (b) bilayer, and (c) coating film. Single particle model (···).

decrease is due to an increase of the minimum, and the second is due to a decrease of the maximum that operates over the previous increase of the minimum.

It has also been observed that if the thickness of the coating film is increased, the maximum becomes more acute. However, this effect should not be confused with the effect caused by a depletion layer. In the cases in which the thickness of the coating film was substantially increased, a notorious effect on the accentuation of the peak was noticed but the single particle profile remained almost unchanged. It could be concluded from this observation that no depletion layer like effect was taking place, but rather an increase in the correlation among the positions of the particles, caused by an enlargement of the pseudoparticles formed by the particle plus its coating film, was responsible of this accentuation of the peak.

Light scattering patterns similar to the ones shown in Figure 7 have been reported in the literature for epoxy−elastomer blends.[3,17] According to our results and without further evidence, these patterns could be easily ascribed to an NG mechanism.

6.1.2. Polydisperse Particles at High Conversions. The full version of the phase separation model that considers the particle-size distribution has been used here.

At low conversions, where the single particle approach is valid, the results were similar to those obtained for the monodisperse case; i.e., the presence of a maximum is not related to the spatial arrangement of the particles. The effect of polydispersity for the single particle approach has already been reported in a previous publication[5] and will not be discussed here. The interest is now focused on the only effect of polydispersity at high conversions where the correlation effect noticed in the monodisperse case could be partially or totally washed out.

In Figure 8 the evolution in real space of part of the sample that is being studied is shown for six values of conversion. The corresponding particle-size distributions are shown in Figure 9. The light scattering patterns are shown in Figure 10 for the same cases as in Figure 7. As can be noticed, the same type of results as in the monodisperse case are obtained. The effect of polydispersity is to partially reduce the interference effect that gives rise to the maximum at $q \neq 0$. However, even though the particle-size distributions are broad, the maximum in the light scattering pattern is still clearly evident.

6.2. Low Volume Fraction of Monodisperse Particles at High Conversions. This case is represented by a formulation with $\phi_{20} = 0.0497$. Again the simplified version of the phase separation model that considers the particles as monodisperse has been used here. Figure 11a shows the predicted trajectory in the conversion vs composition transformation diagram, while parts b and c of Figure 11 represent the evolution of volume fraction of the dispersed phase, particle concentration, and particle radius. The trajectory lies again close to the binodal curve during the whole conversion range.

At low conversions where the single particle approach is valid the results were similar to those obtained in the high volume fraction case above; i.e., the presence of a maximum is not related to the spatial arrangement

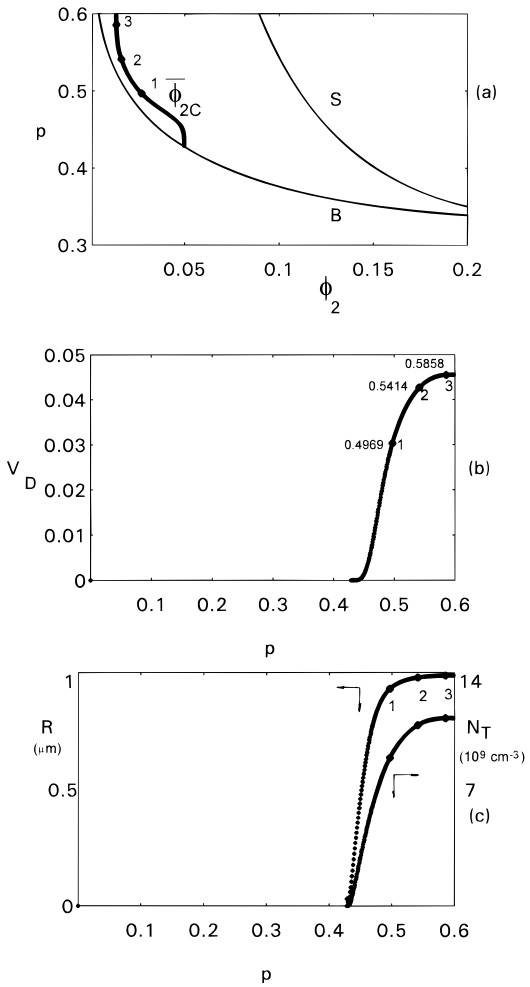

Figure 11. Predictions of the phase separation model for the case of a monodisperse distribution of particle sizes and $\phi_{20} = 0.0497$. (a) evolution of the average composition in the continuous phase; (b) volume fraction of dispersed phase as a function of conversion; (c) particle concentration, N_T (cm^{-3}) and particle radius, R (μm), as a function of conversion.

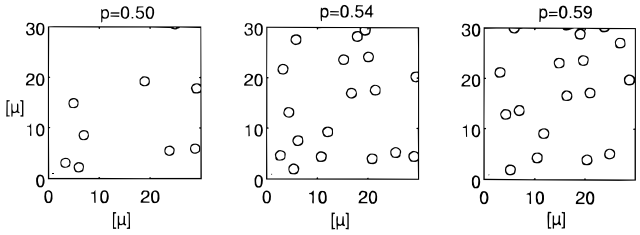

Figure 12. Evolution in real space of the sample for the case of a monodisperse distribution of particle sizes with $\phi_{20} = 0.0497$, high conversions, and low volume fraction of particles, for three different values of conversion.

of the particles. The interest is now focused on the effect of volume fraction of particles at high conversions.

In Figure 12 the evolution in real space of part of the sample that is being studied is shown for three values of conversion. The light scattering profiles corresponding to these samples are shown in Figure 13 for the case of homogeneous particles in a homogeneous medium. The profiles that correspond to a single particle are also shown on the same plot. Apart from the difference always present at values of the wave vector close to zero, only a slight departure of the "real" light scattering profile from the single particle profile is noticed at other wave vector values. This may be explained by the fact

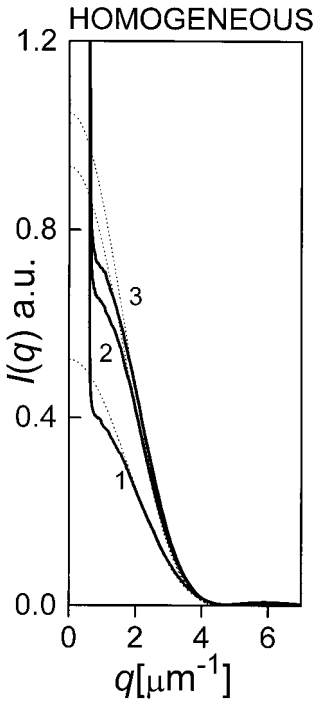

Figure 13. Evolution of the light scattering profiles (—) for the case of a monodisperse distribution of particle sizes with $\phi_{20} = 0.0497$, high conversions, and low volume fraction of particles for three different values of conversion as in Figure 12 for the homogeneous model. Single particle model (···).

that, even at the end of the transformation process, the volume fraction of particles is still low enough that the single particle model may nevertheless be a good approximation, and therefore, a secondary peak at $q \neq 0$ should not necessarily be observed during the course of the transformation.

6.3. Systems under Coalescence or Ostwald Ripening Effects. Factors leading to the presence of a maximum in the scattered light at $q_{max} \neq 0$, are independent of the constitutive equations used in the NG model discussed in section 2; i.e., any model leading to a high concentration of dispersed-phase particles, even with a broad distribution of particle sizes, will determine the existence of a correlation effect among particles and the presence of a maximum in the light scattering pattern.

However, the shift of q_{max} with conversion will depend primarily on the evolution of the concentration of dispersed-phase particles; i.e., q_{max} depends on N_T. In the proposed NG model the coalescence of dispersed-phase particles was considered negligible (in fact, a coalescence term was introduced in eq 7, as in ref 7, and it showed no effect due to the high viscosity of the medium). No other coarsening mechanisms were considered. Therefore, N_T could only increase or attain a constant value when no driving force existed for nucleation due to the proximity of the actual trajectory in the metastable region to the binodal curve (Figure 4).

The presence of coalescence or other coarsening mechanisms will determine a different evolution for N_T. In the late stages of phase separation, droplets evolve so as to minimize their surface-to-volume ratio, thereby minimizing the surface free energy. In this last stage, known as Ostwald ripening or coarsening, the concentration of dispersed-phase particles may be reduced by the Lifshitz−Slyozov mechanism.[18−21] In this case, the ripening is driven by the size dependence of the solubil-

ity of droplets (smaller droplets are dissolved while larger droplets grow). For such a system and assuming the generation of a high volume fraction of particles, light scattering patterns will show a maximum shifting to the left due to the coarsening effect. An example of this behavior has been recently reported for the thermal-induced phase separation in a polymer-dispersed liquid crystal (PDLC).[22] For a particular poly(methyl methacrylate)−LC formulation containing 40 wt % LC, a thermal quench from 80 to 62 °C placed the system in the metastable region of the phase diagram. A droplet structure generated by an NG mechanism was clearly observed by polarized optical microscopy. The average diameter of droplets grew with time while the particle concentration decreased, i.e., coarsening of the distribution was observed.

Light scattering patterns showed the presence of a maximum at $q_{max} \neq 0$, shifting to the left with elapsed time. This constitutes clear experimental evidence of the correlation effect introduced by the presence of a high volume fraction of particles generated by an NG mechanism. This maximum was incorrectly assigned to a diffraction effect.[22] Secondary diffraction maxima are negligible at high volume fractions of particles when compared with maxima resulting from interference, an effect not considered in the analysis by these authors.

7. Conclusions

In this work we have demonstrated that the presence of a maximum in the light scattering pattern of a phase-separating system at a wave vector $q \neq 0$, should not be automatically ascribed to a system undergoing SD. In fact, we have shown, through a fairly comprehensive model, that a system in which phase separation proceeds through an NG mechanism may exhibit the maximum during the whole transformation process. At the beginning, when the volume fraction of particles is low, the maximum may be caused by the presence of a depletion layer that surrounds the particles. At higher volume fractions the increased correlation produced by the location of individual scatterers in a constrained space may be responsible for the presence of the maximum. Besides, the position of the maximum was found to depend on the number of particles per unit volume at high volume fractions, such that q_{max} increases with N_T.

It must be pointed out, however, that the form in which the particles were accommodated, i.e., with all the centers on the same plane, simplifies the computations but overestimates the order in the system. A real three-dimensional simulation will give a closer picture of the light scattering patterns.

We have also discussed the cases in which the maximum is not present and concluded that below some volume fraction of particles in the sample the system behaves as normally expected for systems undergoing decomposition through an NG mechanism; i.e., the light pattern is a monotonically decreasing function of the wave vector. In this case we do not discard the presence of a maximum at the very early stage of the decomposition due to depletion layer effects.

Factors leading to the presence of a maximum in light scattering patterns are independent of the NG-constitutive equations used for the generation of the particle-size distribution. For systems that do not exhibit coarsening effects (i.e., coalescence or Ostwald ripening), the light scattering peak will initially shift to the right and then grow in intensity at a constant value of the wave vector, i.e., when nucleation becomes negligible. Coarsening produces a shift of the scattering peak to the left while increasing its intensity, an effect that was experimentally observed during a thermal quench of a particular polymer-dispersed liquid crystal to the metastable region.[22]

References and Notes

(1) Hashimoto, T. *Phase Transitions* **1988**, *12*, 47.
(2) Inoue, T. *Prog. Polym. Sci.* **1995**, *20*, 119.
(3) Kyu, Th.; Lee, J. H. *Phys. Rev. Lett.* **1996**, *76*, 3746.
(4) Cumming, A.; Wiltzius, P.; Bates, F. S. *Phys. Rev. Lett.* **1990**, *65*, 86.
(5) Eliçabe, G. E.; Larrondo, H. A.; Williams, R. J. J. *Macromolecules* **1997**, *30*, 6550.
(6) The meaning of correlation is here associated with the concept of order. We use the word correlation because it is used in most of the literature, sometimes as a qualitative concept as here, but some other times in a more rigorous manner through precise mathematical definitions.
(7) Williams, R. J. J.; Borrajo, J.; Adabbo, H. E.; Rojas, A. J. In *Rubber-Modified Thermoset Resins; Advances in Chemistry Series* 208; Riew, C. K., Gillham, J. K., Eds.; American Chemical Society: Washington, DC, 1984; p 195.
(8) Vazquez, A.; Rojas, A. J.; Adabbo, H. E.; Borrajo, J.; Williams, R. J. J. *Polymer* **1987**, *28*, 1156.
(9) Moschiar, S. M.; Riccardi, C. C.; Williams, R. J. J.; Verchere, D.; Sautereau, H.; Pascault J. P. *J. Appl. Polym. Sci.* **1991**, *42*, 71
(10) Wolf, B. A.; Heinrich, M. *Polymer* **1992**, *33*, 1926.
(11) Riccardi, C. C.; Williams, R. J. J. *J. Appl. Polym. Sci.* **1986**, *32*, 3445.
(12) Williams, R. J. J.; Rozenberg, B. A.; Pascault, J. P. *Adv. Polym. Sci.* **1997**, *128*, 95.
(13) Jackson, J. D. *Classical Electrodynamics*; John Wiley & Sons: New York, 1975.
(14) Kerker, M. *The Scattering of Light and Other Electromagnetic Radiation*. Academic Press: New York, 1969.
(15) Bohren, C. F.; Huffman, D. R. *Absorption and Scattering of Light by Small Particles;* John Wiley & Sons: New York, 1983.
(16) Tromp, R. H.; Jones, R. A. L. *Macromolecules* **1996**, *29*, 8109.
(17) Baeke, L.; Thioudelet, P.; Keates, P.; Navard, P. *Polymer* **1997**, *38*, 5283.
(18) Lifshitz, I. M.; Slyozov, V. V. *Phys. Chem. Solids* **1961**, *19*, 35.
(19) Wagner, C. *Z. Elektrochem.* **1961**, *65*, 581.
(20) Marqusee, J. A.; Ross, J. *J. Chem. Phys.* **1983**, *79*, 373.
(21) Marqusee, J. A.; Ross, J. *J. Chem. Phys.* **1984**, *80*, 536.
(22) Kyu, T.; Ilies, I.; Shen, C.; Zhou, Z. L. In *Liquid-Crystalline Polymer Systems. Technological Advances;* ACS Symposium Series 632; Isayev, A. I., Kyu, T., Cheng, S. Z. D., Eds.; American Chemical Society: Washington, DC, 1996; p 201.

MA9805304